

Patterned Electrospun Nanofiber Matrices Via Localized Dissolution: Potential for Guided Tissue Formation

*Chao Jia, Dou Yu, Marven Lamarre, Philip L. Leopold, Yang D. Teng, and Hongjun Wang**

With the ability to fabricate sub-micrometer and nanometer fibers from either a melt or a solution, electrospinning has been widely adopted to produce membranes for filtration, catalysis, medicine.^[1] Due to their dimensional similarity to the native tissue extracellular matrix (ECM), electrospun matrices have been explored for versatile applications in regenerative medicine aiming to promote cell–fiber interactions for regulation of cell phenotype,^[2] direct tissue regeneration via contact guidance,^[3] support stem-cell proliferation and differentiation,^[4] and create three-dimensional (3D) tissues with cells encapsulated inside the fibers^[5,6] or embedded among the fibers.^[7] Through modulation of the electric field settings electrospinning can produce distinct fiber arrangements^[8] and, therefore, form anisotropic fibrous matrices. One of the most common approaches is to manipulate the topographical features of fiber collecting surfaces,^[9,10] which alters the distribution of electric intensity and consequently modulates fiber deposition, e.g., collecting electrospun fibers onto a rotating mandrel leads to parallel fiber organization.^[11] Evidence has increasingly suggested that such anisotropic fiber organizations induce cell elongation, promote cell migration, and regulate cell differentiation via integrin-mediated outside-in signaling.^[12] Building various anisotropic features into electrospun matrices^[13–16] is highly desirable because of its potential to better mimic the unique mechanical and biologic functions of tissue ECM and consequently guide preferred tissue formation. However, current electric field intervention tactics can only modulate the fiber arrangement without feasibility of accommodating many other hierarchical and complex characteristics of native tissues (e.g., various patterned organization of cells). To this end, some pioneering efforts have been made to electrospin cells encapsulated within biopolymeric fibers into 3D structures.^[5,6] While being recognized for the advantages, its application is limited to several particular materials. Hence, it is of great benefit to develop a cost-effective technology platform enabling the creation of arbitrary patterns in electrospun fiber matrices for

patterned distribution of cells with intricate arrangements and corresponding cellular responses.

Herein we present an innovative approach, an inkjet-printer based printing of solvent onto electrospun fiber meshes to selectively dissolve nanofibers for creating various patterns without sacrificing the superior properties of electrospun fibers. Specifically, AutoCAD designed patterns are the “files” for printing, the solvent loaded in the printer cartridge is used as “ink” and electrospun fiber meshes are used as “paper”. During printing, the solvent precisely deposited by the printer dissolves the contacted fibers to generate pores, while the dissolved nanofibers of printed area fuse into thicker fibers or solidify on the rim of the unprinted areas to form stable patterns.

Cells (endothelial cells, fibroblasts and neural cells) cultured on the printed meshes exhibited a similar distribution pattern to the remaining fibers where they preferably attached. This technology allows for the fabrication of different patterns containing microfiber and nanofiber depending on the designated patterns and related parameters, such as the solvent solubility, fiber mesh thickness, drop-to-drop distance (DD) and piezoelectric voltage controlled single drop size (DS). Compared to those collecting surface-modulated patterning and lithography approaches,^[10,17,18] this inkjet printer-enabled localized nanofiber dissolution offers high resolution (e.g., DS is as small as 5 pL and printing area size is as small as 50 μm in diameter), high reproducibility and diversified patterns. This suggests that localized dissolution-patterned electrospun meshes has many potential multifaceted applications, such as differential regulation of the proliferation of human neural stem cells (hNSCs) by unprinted nanofiber area and guided neurite extension by printed microfibers on the same meshes.

Electrospun fiber meshes of blended 8% w/v polycaprolactone (PCL) and 8% w/v collagen in hexafluoroisopropanol (HFIP) were chosen as “print paper” based on their mechanical strength^[19] and the biologic functions of collagen for supporting the attachment and growth of several types of cells.^[20] With our established electrospinning conditions, nanofibers with diameters of 200–500 nm^[7] were obtained and collected onto a grounded circular metal ring in a random fashion. Under fixed electrospinning conditions, the thickness of nanofiber meshes was a function of the collection time and collection for 4 min gave a thickness of $15.7 \pm 0.7 \mu\text{m}$ in our experimental setup (Figure S1, Supporting Information). Importantly, the mesh thickness correlated with the amount of solvent needed for dissolving. For example, when using HFIP as solvent, a thickness of up to 20 μm was still optimal, i.e., the mesh was effectively dissolved by the smallest DS of 5 pL without losing mechanical integrity. However, the amount of dissolved polymer was too

C. Jia, M. Lamarre, Prof. P. L. Leopold, Prof. H. Wang
Chemistry, Chemical Biology
and Biomedical Engineering
Stevens Institute of Technology
1 Castle Point on Hudson, Hoboken, NJ 07030, USA
E-mail: Hongjun.wang@stevens.edu

Dr. D. Yu, Prof. Y. D. Teng
Department of Neurosurgery
Brigham and Women's Hospital and Division of SCI Research
VA Boston Healthcare System
Harvard Medical School
221 Longwood Avenue, Boston, MA 02115, USA

DOI: 10.1002/adma.201403509



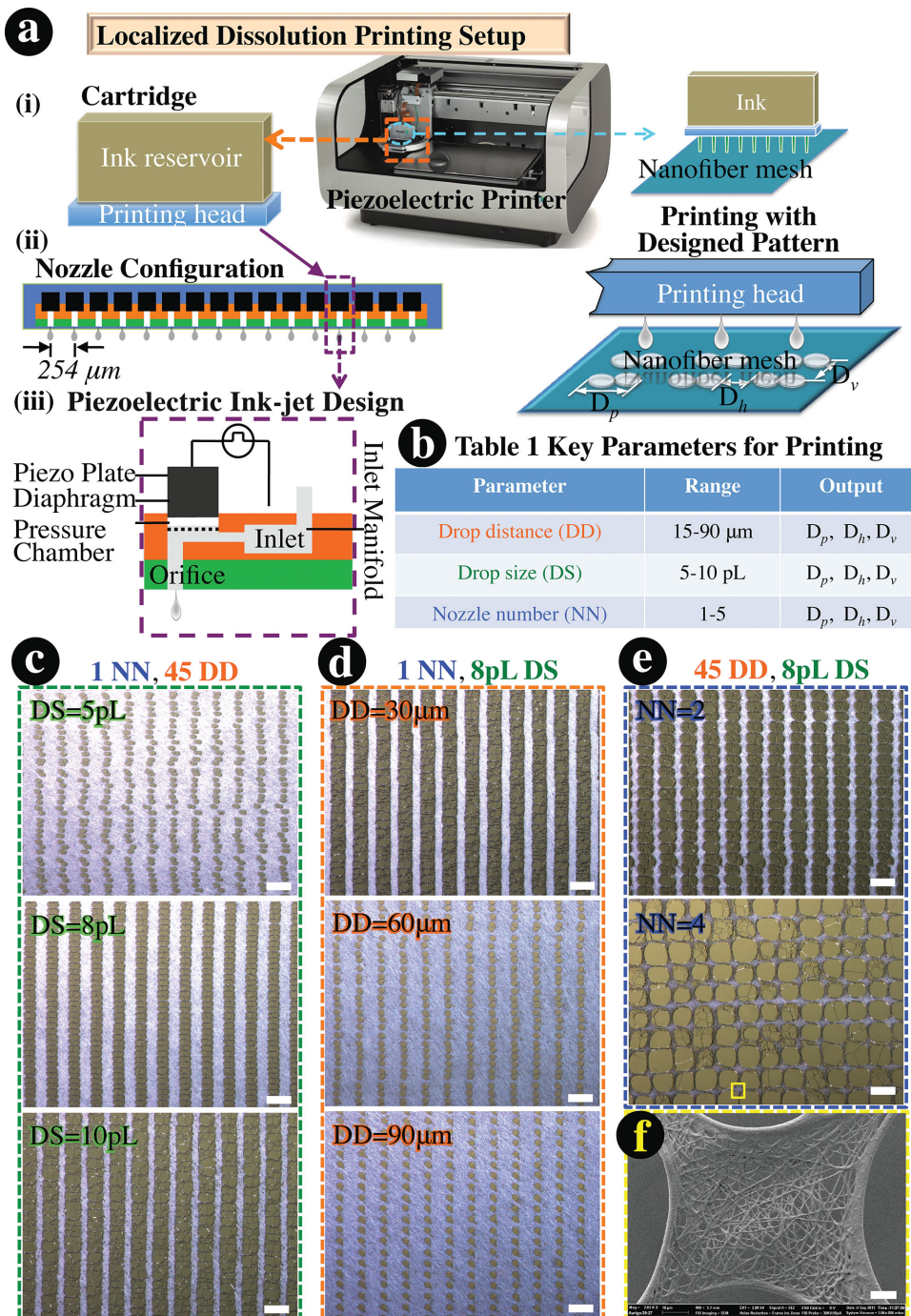


Figure 1. a) Schematic illustration of the localized nanofiber dissolution setup featuring the cartridge (i) with 16-nozzle printing head (ii), which are individually powered by the piezoelectric jet system (iii). The piezoelectric ink-jet design allows pushing the solvent drops out of the cartridge by electrical charge-generated pressure and then printing them onto the nanofiber meshes (i). b) The key parameters including drop-to-drop distance (DD), drop size (DS), and nozzle number (NN) influence the printing output, which are characterized by D_p , D_h and D_v . c – e) Stereomicroscopy images of resulted patterns with different parameters. Input AutoCAD pattern is parallel stripes with alternative printed (width = 90 μm) and unprinted areas (width = 90 μm). Different parameters are highlighted in different colors: DS: green; DD: orange; NN: blue. Scale bar: 200 μm. f) SEM micrograph of the marked area of (e) shows the unprinted area still remains their nanofiber morphology except the fused edges. Scale bar: 10 μm.

high to fuse only to the rim of the printed areas and started to form dense membrane (Figure S2, Supporting Information).

In contrast to the extensive use of Dimatix Materials Printer DMP-2800 for fabricating 3D structures from various

polymers,^[21-23] the piezoelectric drop-on-demand ink-jetting platform of the printer was adopted for printing HFIP onto electrospun PCL/collagen fiber meshes in our design (Figure 1a). Although other solvents could be used, e.g.,

chloroform or dichloromethane (DCM), HFIP was chosen because of its solubility to both PCL and collagen and the moderate evaporation rate (Figure S3, Supporting Information). Different from printing polymer solutions with high viscosity and low flow rate, printing volatile and highly diffusible HFIP represents a great challenge. Several key parameters, including DS, DD and nozzle number (NN), were identified and evaluated for their contribution to the printing accuracy of designed patterns (Figure 1b). Two major criteria are considered for optimizing the printing conditions: 1) the solvent drops should be big enough to efficiently dissolve the desired area of fibers, and 2) excessive-diffusion of solvents as a result of the untimely evaporation should be minimized to maintain a high resolution. To better understand the process of HFIP-assisted printing, 1% (w/v) fluorescein isothiocyanate (FITC)-labeled bovine serum albumin (BSA) was included in HFIP for printing, allowing us to visualize the diffusion of solvent and the distribution of HFIP-dissolved nanofibers. Interestingly, upon HFIP evaporation, the printed area exhibited a fluorescent ring with distinct halo (Figure S4a,b, Supporting Information). Comparison with bright-field images (Figure S4c,d, Supporting Information) indicated that the halo (i.e., diffusion zone) might come from the diffusion of solvent without obvious nanofiber dissolution, and the intensive inner fluorescent circle (i.e., fusion zone) was a result of the fusion of dissolved nanofibers. Indeed, close examination of the fusion zone by SEM did show a dense rim structure (Figure S4d inset, Supporting Information). Based on the result, when using 8 pL DS, 45 μm DD and 1 NN, the resulted pattern most accurately reproduced the input pattern. Depending on the voltage from 15 to 40 mV, DS could be tuned from 5 to 10 pL. During printing, the area of fibrous meshes dissolved by solvent drop was closely correlated with DS (Figure 1c). For example, a dissolved area of $48.6 \pm 0.8 \mu\text{m}$ in diameter was normally observed with one 8 pL DS (30 mV voltage) drop. As a consequence, both pore size (D_p) and intact mesh width (horizontal distance D_h and vertical distance D_v) was a linear function of DS (Table S1 and Figure S5, Supporting Information). Within a selected DD range of 15–90 μm, it was found that DD larger than 60 μm led to a discrete printing whereas 45 μm DD was sufficient to yield a continuous printing (Figure 1d). With the increase of DD from 15 to 60 μm, D_p exhibited a second-order polynomial decrease and D_h showed an exponential increase (Table S1 and Figure S5, Supporting Information). To better maintain the desired patterns and avoid excessive dissolution of nanofibers by solvent, one nozzle was used for the rest of the study (Table S1, Supporting Information). It is necessary to mention that despite a noted fusion at the edge of unprinted regions a majority of the intact nanofibers retain their random organization, similar to that prior to printing (Figure 1f).

With optimized conditions (8 pL DS, 45 DD, 1 NN and HFIP), we first investigated whether localized nanofiber dissolution could be used to create one-dimensional patterns by printing parallel stripes with various designated widths (Figure 2a). The resulting patterns displayed distinct variation in morphology over the graded increase of the width. For the designated widths of 10, 30, and 50 μm, printing did not create stripes; instead it yielded a network of parallel thick microfibers (ca. 20 μm in diameter), perpendicular to the designated stripe

direction and interconnected by thin microfibers (ca. 3 μm in diameter) (Figure 2b). This finding demonstrated the possibility of creating a fibrous network composed solely of microfibers with controllable fiber-to-fiber distance. Under the current printing condition, one drop of solvent will create an approximately 50 μm hole on the mesh. When the unprinted area width fell into this range (e.g., 10–50 μm), nanofibers along the stripe direction would be completely dissolved without formation of stripes. The remaining fiber bundles perpendicular to the stripe direction would fuse to form parallel microfibers (see Figure 1c, DS = 10 pL pattern). For those printings with an unprinted width larger than or equal to 100 μm, stripes were formed with a corresponding increase in stripe width (Figure 2b). The resulting stripe width was 98.9 ± 2.9 , 199.8 ± 3.7 , and $502.1 \pm 4.2 \mu\text{m}$ for the 100, 200 and 500 μm design, respectively, indicating a good printing resolution. To further determine whether the printed patterns were also related to the printing direction, a square spiral with the same printed and unprinted width of 100 μm was designed and printed on random fiber meshes (Figure 2c). Clearly, the printing direction significantly affected the resulting patterns (Figure 2d). This observation further suggests the possibility of generating a spatial anisotropy even within the same pattern.

One of the most important advantages in using the inkjet-printing system is its potential to reproduce various patterns.^[24] Despite its success in fabricating polymeric structures,^[25] it remains unclear whether inkjet printer-enabled solvent printing can repeatedly produce identical patterns on the same mesh or different meshes, which is highly desirable for inducing comparable cellular responses within similar patterns and leading to the formation of tissues with identical functions. In this regard, we first explored the possibility of creating similar patterns on the same mesh. An array of concentric circle patterns (6×6) with the width of unprinted and printed area of 50 μm was designed and printed onto nanofiber meshes (Figure S6a(i), Supporting Information). The resulting pattern highly reproduced the input pattern in terms of the remaining nanofiber area as well as the organization of fused microfiber networks in both row and column direction (Figure S6a(ii), Supporting Information). Further increase of the width of both unprinted and printed area in the designed patterns to 100 μm led to the resulting pattern similar to the design (Figure S6b, Supporting Information). We also designed an array of circular patterns (4×4) with the unprinted area width of 2000 μm and printed the patterns onto two separate meshes [Figure S6c(ii) and S6c(iii), Supporting Information] prepared on different days. Based on the measurement of D1 and D2 as indicated in Figure S6c [D1 (ii): $1092 \pm 46 \mu\text{m}$ vs D1 (iii): $1060 \pm 35 \mu\text{m}$, Student's t-test, $p = 0.09$; D2 (ii): $1885 \pm 47 \mu\text{m}$ vs D2 (iii): $1918 \pm 75 \mu\text{m}$, Student's t-test, $p = 0.24$], no significant difference was observed. This result confirms that localized nanofiber dissolution indeed yielded satisfactory resolution with high reproducibility.

Early studies have shown the supportiveness of electrospun PCL/collagen fiber meshes for adhesion and proliferation of several types of cells including endothelial cells and fibroblasts.^[26,27] In addition, increasing evidence highlights the correlation between geometrical dimensions of the substrates and cell morphology as well as their functions.^[28] Accordingly,

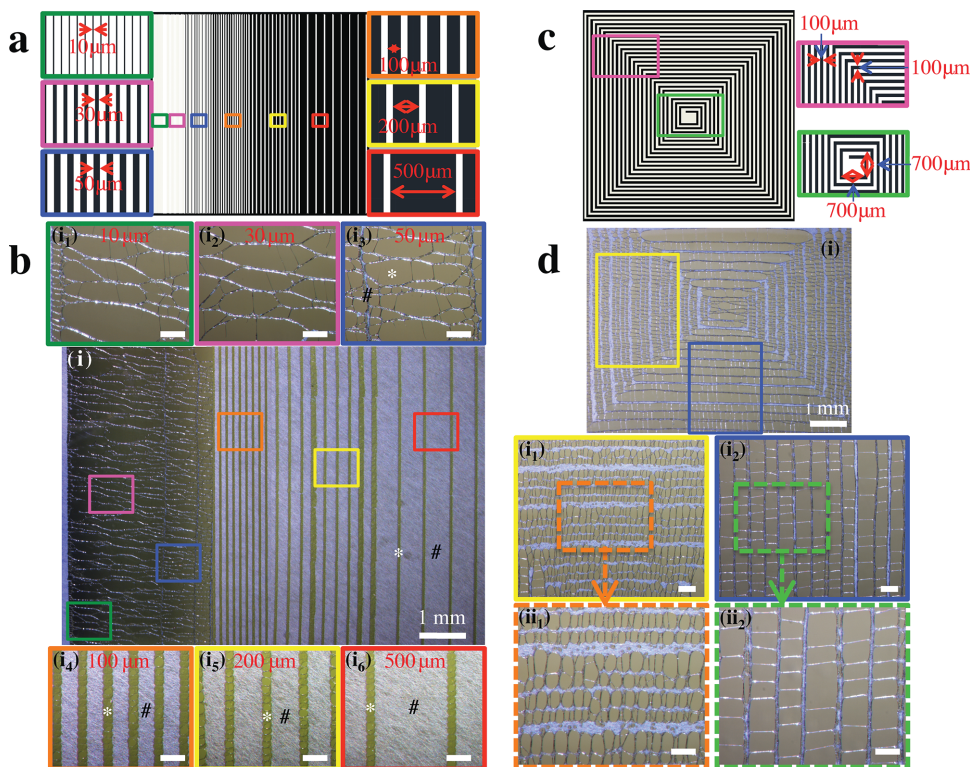


Figure 2. a-d) Inputting AutoCAD patterns and the resulting patterns using localized nanofiber dissolution. a) Inputting AutoCAD pattern of parallel stripes with the same printing width (white) (width = 60 μm) and different unprinted widths (black). Different areas are labeled with different colored boxes. b) i). Stereomicroscopy images of the resulting patterns. The different colors showed magnified images of printing patterns with different unprinted widths: (i₁) green: 10 μm ; (i₂) pink: 30 μm ; (i₃) blue: 50 μm ; (i₄) orange: 100 μm ; (i₅) yellow: 200 μm ; and (i₆) red: 500 μm . The white asterisk (*) indicates the printed area and black hash symbol (#) indicates the unprinted area. c) Inputting AutoCAD pattern of a spiral square with the same printing width (white) (width = 100 μm) and unprinted width (black) (width = 100 μm). d) Stereomicroscopy images of the resulting patterns show distinct morphology in two different printing directions. The images with the colored borders show the magnified images: (i₁) yellow: vertical direction printing; (i₂) blue: horizontal direction printing; (ii₁) orange dash: magnified image of vertical direction printing; (ii₂) green dash: magnified image of horizontal direction printing. Scale bar: 200 μm unless stated otherwise.

localized nanofiber dissolution-patterned nanofiber meshes may also induce differential cell organization with a close correspondence to the printed patterns. Nanofiber meshes with an array of concentric circle patterns (**Figure 3a**) were fabricated and seeded with mouse endothelial cells (MS-1, pancreatic islet endothelial cell line, ATCC, CRL-2279). It was found that the cells closely followed the printed patterns by only attaching to the material surface (i.e., unprinted nanofiber areas and microfiber networks) (**Figure 3b**). On the large intact mesh area, the cells exhibited a random arrangement without preferred orientation (**Figure 3b(i)** and **3b(ii)**), however on the narrow stripes (<100 μm in width) and microfibers (ca. 20 μm in diameter), cells preferentially oriented in the same direction as stripes or microfibers (**Figure 3b(iii)**). This became even more pronounced with microfibers, along which the cells elongated and connected to other cells of the unprinted area (**Figure 3b(iii,iv)**). This result is consistent with previous findings that microgrooved patterns with groove widths less than 100 μm could direct cell alignment and elongation.^[29] A better demonstration of spatially controlled cell morphology was observed with one-dimensional printed stripe patterns (**Figure 2** and **Figure S7**, Supporting Information). Taken together, it is contact guidance^[30] that primarily regulates the spatial distribution

and morphology difference of mouse endothelial cells. Pattern-induced morphology and distribution of human primary dermal fibroblasts were also similarly observed, see **Figure S8** (Supporting Information), in which cells elongated along the printed microfibers while exhibiting disorganized spreading on the intact mesh area.

To further elaborate the utility of patterned PCL/collagen fiber meshes, especially for their regulation of cellular functions, we cultured hNSCs (HFB2050 cells that have been characterized as previously described^[31]) onto printed meshes with segregated domains of small and large pores (**Figure 4a**). Under the same printing parameters, the left portion of the mesh was printed with 200 μm unprinted width and 50 μm printed width to generate small isolated pores (**Figure 4a(i)**), and the right portion was printed with 50 μm unprinted width and 50 μm printed width to dissolve away a majority of nanofibers for large pores along with the formation of bridging microfibers (**Figure 4a(ii)**). It was found that intact nanofiber supported the attachment and proliferation of hNSCs in their progenitor status. The colonies of hNSCs in the small pore domain (red circles) were much smaller with shorter neurites than those in the large pore domain that appeared discernibly larger with longer neurites (blue circles) (**Figure 4b(i)**). This observation

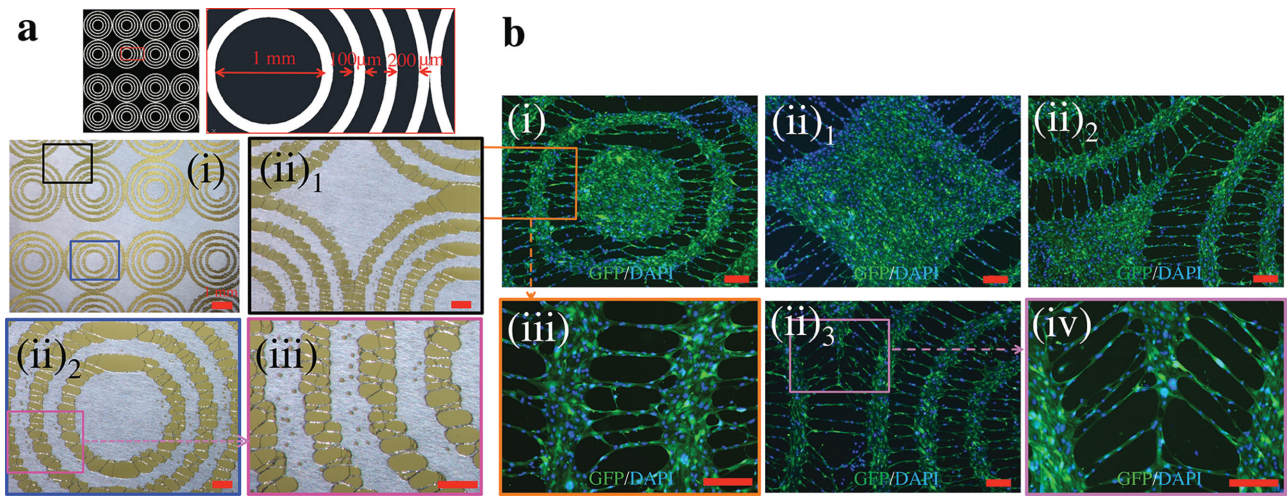


Figure 3. a,b) Creation of concentric circles on nanofiber meshes and their regulation of cell distribution. a) The inputting AutoCAD pattern of concentric circles with printed area (white) (width = 100 μm) and unprinted area (black) (width = 200 μm) leads to the pattern formation as visualized by stereomicroscopy (i–iii). i) Overview of the printed patterns on nanofiber meshes. ii₁) Magnified image of the blue box area. ii₂) Magnified image of the black box area. iii) Magnified image of the pink box area in (ii₂). Scale bar: 200 μm unless stated otherwise. b) Fluorescence images of GFP⁺ MS-1 cells cultured on the pattern for 3 days, showing that the cell distribution closely follows the printed pattern and the cell morphology is regulated by the matrix dimensions (i–iv). Cell nuclei were stained blue by 4',6-diamidino-2-phenylindole (DAPI). i) The concentric circle area. ii_{1–3}) Three different areas between two concentric circle patterns. iii) Magnified image of the orange box area in (i). iv) Magnified image of the purple box area in (ii₃). Scale bar: 200 μm .

suggests that hNSCs in the smaller pore domain have a better migratory capability, preventing the formation of large colonies. Upon deprivation of trophic/mitotic factors, noticeable induction of neural phenotypic differentiation^[32] was observed at

both domains by strong expression of neural filament M (NFM, green; neuronal marker) (Figure 4b(iii), 4b(iv)) and high expression of TUJ1 (red; early neuronal marker) in all cell colonies (Figure 4b(v), 4b(iv)). Deprivation of the trophic/mitotic factors

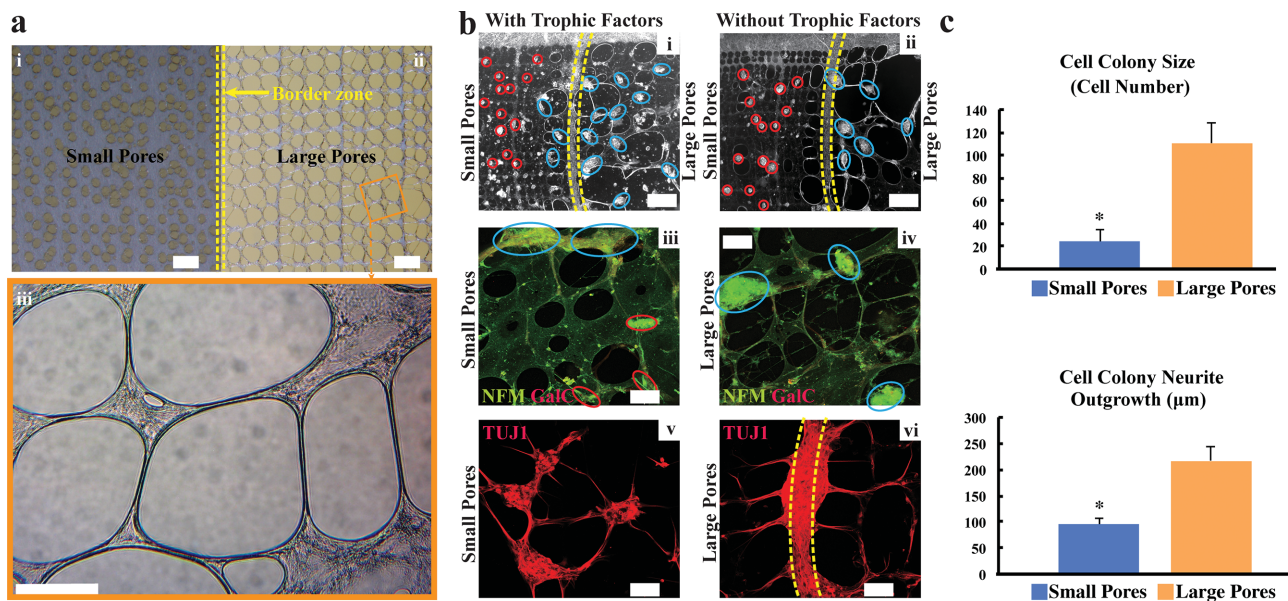


Figure 4. a–c) Culture of hNSCs on two different printed nanofiber meshes. a) Nanofiber meshes with dual printed domains, i.e., small pore (i) and large pore (ii) (divided by yellow broken lines), was fabricated based on two distinct AutoCAD inputs. i,ii) Stereomicroscopy images; iii) inverted microscopy images show microfibers connecting the intact nanofiber area in the large pore domains (orange box area in (a_{ii})). b) Microscopy images of hNSCs cultured on both patterned domains show strong expression of NFM (green; neuronal marker) in cells (iii) and (iv) and high expression of TUJ1 (red; early neuronal marker) in all the cell colonies (v) and (vi). c) Quantitative analysis ($n = 14/\text{each pore area}$) shows that printed domains with larger pores significantly nurture bigger cell colonies [111 ± 17 cells per colony (large pore) vs 24 ± 2 cells per colony (small pore)] and longer distance of neurite outgrowth [$217 \pm 27 \mu\text{m}$ (large pore) vs $94 \pm 11 \mu\text{m}$ (small pore); * $p < 0.05$]. Scale bar: 100 μm .

did not alter cell attachment profile on both porous domains (Figure 4b(ii)). Although both patterns supported neural differentiation, neurite extensions, important to form neuronal networks,^[33,34] were much longer for cells cultured on the large pore domains relative to those of cells on the small pore domains and the outgrowth of neurites followed the microfiber contours of the large pore domains (Figure 4b(v) vs 4b(iv)), suggesting the guiding role of bridging microfibers in neurite outgrowth. Quantitative analysis further confirmed that patterned meshes with large pores significantly nurtured larger cell colonies (Figure 4c).

In summary, localized nanofiber dissolution offers a unique avenue for a rapid and reproducible modification of electrospun fiber meshes with versatile patterns, which not only enable the spatial organization of cells with anisotropy and complexity, but also differentially regulate their differentiation within the same mesh. In addition, the ability to create large open pores through dense electrospun fiber meshes using the localized nanofiber dissolution can also cost-effectively address the significant challenges in limited cell infiltration and tissue ingrowth with current electrospun meshes.^[35] With the capabilities of tuning the composition of nanofibers, printing drug-eluting micropatterns on nanofiber meshes for local release of biomolecules (e.g., growth factors and cytokines),^[36] localized nanofiber dissolution to form arbitrary patterns in nanofiber meshes, and layer-by-layer assembly of cell-seeded nanofiber meshes into 3D constructs,^[7] it is feasible for electrospun fibers to capture the versatile features of native ECM and guide 3D desired tissue formation.

Experimental Section

Experimental details are available in the Supporting Information.

Supporting Information

Supporting Information is available from the Wiley Online Library or from the authors.

Acknowledgements

The authors are grateful for the technical assistance from Mr. Yixin Gu and Dr. Tsengming Chou in SEM examination. Special thanks are also given to Dr. Shaohua Li (Rutgers-Robert Wood Johnson, NJ, USA), who provided GFP transfection to the mouse endothelial cells. Part of the work was financially supported by NSF-IIP (1338958, 1346430, Wang), NSF-CBET (1033742, Wang), NIAMS (1R21 AR056416, Wang), VARR&D (Teng) and CIMIT-DoD (Teng).

Received: August 1, 2014

Revised: September 16, 2014

Published online: October 28, 2014

[1] A. Greiner, J. H. Wendorff, *Angew. Chem. Int. Ed. Engl.* **2007**, *46*, 5670.

- [2] W. J. Li, C. T. Laurencin, E. J. Caterson, R. S. Tuan, F. K. Ko, *J. Biomed. Mater. Res.* **2002**, *60*, 613.
- [3] L. Zhang, T. J. Webster, *Nano Today* **2009**, *4*, 66.
- [4] X. Xin, M. Hussain, J. J. Mao, *Biomaterials* **2007**, *28*, 316.
- [5] A. Townsend-Nicholson, S. N. Jayasinghe, *Biomacromolecules* **2006**, *7*, 3364.
- [6] S. N. Jayasinghe, *Analyst* **2013**, *138*, 2215.
- [7] X. Yang, J. D. Shah, H. Wang, *Tissue Eng., Part A* **2009**, *15*, 945.
- [8] D. Li, Y. Xia, *Adv. Mater.* **2004**, *16*, 1151.
- [9] W. Liu, S. Thomopoulos, Y. Xia, *Adv. Healthcare Mater.* **2012**, *1*, 10.
- [10] D. Zhang, J. Chang, *Adv. Mater.* **2007**, *19*, 3664.
- [11] P. Katta, M. Alessandro, R. D. Ramsier, G. G. Chase, *Nano Lett.* **2004**, *4*, 2215.
- [12] C. Huang, X. Fu, J. Liu, Y. Qi, S. Li, H. Wang, *Biomaterials* **2012**, *33*, 1791.
- [13] G. R. Mitchell, A. Tojeira, *Proc. Eng.* **2013**, *59*, 117.
- [14] H. G. Senel-Ayaz, A. Perets, M. Govindaraj, D. Brookstein, P. I. Lelkes, *Conf. Proc. IEEE Eng. Med. Biol. Soc.* **2010**, *2010*, 255.
- [15] H. G. Senel Ayaz, A. Perets, H. Ayaz, K. D. Gilroy, M. Govindaraj, D. Brookstein, P. I. Lelkes, *Biomaterials* **2014**.
- [16] M. Park, J. Im, J. Park, U. Jeong, *ACS Appl. Mater. Interfaces* **2013**, *5*, 8766.
- [17] X. Xia, S. Xie, M. Liu, H. C. Peng, N. Lu, J. Wang, M. J. Kim, Y. Xia, *Proc. Natl. Acad. Sci. USA* **2013**, *110*, 6669.
- [18] J. Xie, W. Liu, M. R. MacEwan, Y. C. Yeh, S. Thomopoulos, Y. Xia, *Small* **2011**, *7*, 293.
- [19] J. Johnson, A. Niehaus, S. Nichols, D. Lee, J. Koepsel, D. Anderson, J. Lannutti, *J. Biomater. Sci., Polym. Ed.* **2009**, *20*, 467.
- [20] J. S. Choi, S. J. Lee, G. J. Christ, A. Atala, J. J. Yoo, *Biomaterials* **2008**, *29*, 2899.
- [21] B. J. de Gans, P. C. Duineveld, U. S. Schubert, *Adv. Mater.* **2004**, *16*, 203.
- [22] L. Pan, G. Yu, D. Zhai, H. R. Lee, W. Zhao, N. Liu, H. Wang, B. C. Tee, Y. Shi, Y. Cui, Z. Bao, *Proc. Natl. Acad. Sci. USA* **2012**, *109*, 9287.
- [23] S. F. Jahn, L. Engisch, R. R. Baumann, S. Ebert, W. A. Goedel, *Langmuir* **2009**, *25*, 606.
- [24] A. Bietsch, J. Zhang, M. Hegner, H. P. Lang, C. Gerber, *Nanotechnology* **2004**, *15*, 873.
- [25] B. J. de Gans, U. S. Schubert, *Langmuir* **2004**, *20*, 7789.
- [26] S. J. Lee, J. J. Yoo, G. J. Lim, A. Atala, J. Stitzel, *J. Biomed. Mater. Res. A* **2007**, *83*, 999.
- [27] E. Schnell, K. Klinkhammer, S. Balzer, G. Brook, D. Klee, P. Dalton, J. Mey, *Biomaterials* **2007**, *28*, 3012.
- [28] V. Vogel, M. Sheetz, *Nat. Rev. Mol. Cell Biol.* **2006**, *7*, 265.
- [29] A. Kapoor, E. H. Caporali, P. J. Kenis, M. C. Stewart, *Acta Biomater.* **2010**, *6*, 2580.
- [30] A. I. Teixeira, G. A. Abrams, P. J. Bertics, C. J. Murphy, P. F. Nealey, *J. Cell Sci.* **2003**, *116*, 1881.
- [31] Y. D. Teng, S. C. Benn, S. N. Kalkanis, J. M. Shefner, R. C. Onario, B. Cheng, M. B. Lachyankar, M. Marconi, J. Li, D. Yu, I. Han, N. J. Maragakis, J. Llado, K. Erkmen, D. E. Redmond, Jr., R. L. Sidman, S. Przedborski, J. D. Rothstein, R. H. Brown, Jr., E. Y. Snyder, *Sci. Transl. Med.* **2012**, *4*, 165ra164.
- [32] J. Wagner, P. Akerud, D. S. Castro, P. C. Holm, J. M. Canals, E. Y. Snyder, T. Perlmann, E. Arenas, *Nat. Biotechnol.* **1999**, *17*, 653.
- [33] P. Walicke, W. M. Cowan, N. Ueno, A. Baird, R. Guillemin, *Proc. Natl. Acad. Sci. USA* **1986**, *83*, 3012.
- [34] M. J. Mahoney, K. S. Anseth, *Biomaterials* **2006**, *27*, 2265.
- [35] Q. P. Pham, U. Sharma, A. G. Mikos, *Biomacromolecules* **2006**, *7*, 2796.
- [36] X. N. Chen, Y. X. Gu, J. H. Lee, W. Y. Lee, H. J. Wang, *Eur. Cells Mater* **2012**, *24*, 237.